

Electronic Supporting Information

Selective surface functionalization generating site-isolated Ir on MnO_x/N-doped carbon composite for robust electrocatalytic water oxidation

Ning Yan ^{a*}, Remko J. Detz ^{a,b}, Nitish Govindarajan^a, Jacobus M. Koelewijn ^a, Bin Hua ^c, Peng Li ^d, Evert Jan Meijer ^a, Joost N. H. Reek ^{a*}

^a Van't Hoff Institute for Molecular Sciences, University of Amsterdam, Science Park 904, 1098 XH Amsterdam, The Netherlands. Email: n.yan@uva.nl (N.Y.), j.n.h.reek@uva.nl (J.N.H.R)

^b Energy Transition Studies, ECN part of TNO, Radarweg 60, 1043 NT Amsterdam, The Netherlands

^c Department of Chemical and Materials Engineering, University of Alberta, T6G 1H9, Edmonton, Alberta, Canada

^d NanoFAB Centre, University of Alberta. T6G 2V4, Edmonton, Alberta, Canada

Experimental

1. Synthesis of MnO_x/N-C nanorod.

The detailed synthesis procedure of MnO_x/N-C nanorod hybrid was reported in our previous work. In brief, the hybrid was prepared using a hydrothermal reaction starting from manganese acetate and nitrotriactic acid. The reaction was performed at 180 °C for 6 h, the subsequently obtained white powder was sequentially dried, pyrolyzed at 900 °C in argon. The yield of MnO/N-C was finally calcined in air at 200 °C to produce the MnO_x/N-C nanorod containing ~20 wt% N-C and ~80 wt% MnO_x.

2. Synthesis of complex 2.

All chemicals were purchased from commercial suppliers and used without further purification. All syntheses were carried out under a N₂ atmosphere using standard Schlenk techniques unless stated otherwise. CH₂Cl₂ was distilled from sodium. Acetonitrile was distilled from calcium hydride. Nuclear magnetic resonance (NMR) spectra were recorded on a Bruker AMX 400 (400.1 MHz, 100.6 MHz for ¹H and ¹³C respectively) or Bruker Avance 500 (125.78 MHz for ¹³C), which provides a definitive method to identify molecular structure of the obtained organic compounds. The crystal structure is also analyzed using the single-crystal XRD. The obtained molecular structure is shown in Table S1, Figure S1 and S2. The interpretation approach of NMR spectra could be found in Prof. Horst Friebolin's book "Basic One- and Two-Dimensional NMR Spectroscopy" (ISBN: 978-3-527-32782-9).

Synthesis of 1-methyl-3-(trimethoxysilylpropyl)-imidazolium chloride – 23 mL (125 mmol, 1 equiv) (3-chloropropyl)trimethoxysilane was dissolved in 10 mL (125 mmol, 1 equiv) *N*-methyl imidazole in a 50 mL Schlenk flask equipped with a magnetic stirring bar under dry and inert conditions. The mixture was stirred and heated to 70 °C for 72 h at which point the mixture became too viscous to be stirred. After cooling down to room temperature, the viscous oil was vigorously stirred and washed with Et₂O (5x). After drying in vacuum for 24 hours, the ionic liquid 1-methyl-3-(trimethoxysilylpropyl)-imidazolium chloride was obtained quantitatively.

¹H-NMR (400 MHz, CDCl₃): δ = 10.24 (s, 1H), 7.72 (t, 1H), 7.42 (t, 1H), 4.15 (t, 2H), 3.94 (s, 3H), 3.35 (s, 9H), 1.81 (m, 2H), 0.44 (t, 2H); ¹³C-NMR (101 MHz, CDCl₃) 136.7, 123.3, 121.4, 50.8, 49.9, 35.7, 23.4, 5.1.

Synthesis of complex 2 – In a 25 mL Schlenk flask equipped with a magnetic stirring bar was dissolved 150 mg (0.53 mmol, 2 equiv) 1-methyl-3-(trimethoxysilylpropyl)-imidazolium chloride in 10 mL CH₂Cl₂. 75 mg (0.32 mmol, 1.2 equiv) Ag₂O was added and the reaction was stirred for 16 h at room temperature. The addition of Ag₂O assists the deprotonation and metalation to generate the *N*-heterocyclic carbene. 213 mg (0.26 mmol, 1 equiv) (IrCp*Cl₂)₂ was added thereby instantly changing the color of the reaction mixture to yellow. The reaction mixture was left to stir for 30 minutes and filtered over Celite. The clear yellow/orange solution was concentrated to a small

volume which was then added dropwise to the vortex of a 300 mL vigorously stirring pentane solution in a 500 mL round-bottom flask. The yellow amorphous solid flakes were isolated to yield 135 mg of complex **2** (yield 40%). Yellow needle shaped crystals of complex **2** were obtained by diffusion of pentane carefully layered into a concentrated solution of complex **2** in CH₂Cl₂.

¹H-NMR (500 MHz, CDCl₃): δ = 6.98 (d, 2H, NHC), 6.92 (d, 2H, NHC), 4.63 (m, 1H, (CH₃O)₃SiCH₂CH₂CH₂), 3.96 (s, 3H, NHC-CH₃), 3.76 (m, 1H, (CH₃O)₃SiCH₂CH₂CH₂), 3.57 (s, 9H, (CH₃O)₃SiR), 2.11 (m, 1H, (CH₃O)₃SiCH₂CH₂CH₂), 1.82 (m, 1H, (CH₃O)₃SiCH₂CH₂CH₂), 1.60 (15H, Cp*), 0.82-0.65 (m, 2H, (CH₃O)₃SiCH₂CH₂CH₂); ¹³C-NMR APT (125 MHz, CDCl₃) 156.1, 123.5, 121.2, 88.7, 53.1, 50.8, 38.6, 25.4, 9.23, 6.4.

3. Preparation of site-isolated Ir

The immobilization of complex **2** was performed in a 10 mL flask equipped with a magnetic stirring bar, complex **2** was dissolved 0.64 mg (1.0 μmol, 1 mM) in 1 mL CH₃CN. 50 mg of the supports (either MnO_x/N-C or commercial fluorine-doped tin oxide nanoparticles, FTO) was added and the reaction was stirred for 16 h at room temperature. After settlement of the powder, the solvent was removed and the powder was subsequently washed with water (2 mL, 2x) and dried under a gentle stream of nitrogen. The preparation of the control was carried out using a standard impregnation approach. Deionized water and 50 mg of MnO_x/N-C was added to a round-bottom flask that was kept at 60 °C. Under mild agitation, aqueous H₂IrCl₆ (1.0 μmol, 1 mM) solution was added to the flask dropwise. After the evaporation of water, the dried power was retrieved.

To obtain the final site-isolated Ir species, a pyrolysis step was applied to decompose the precursors. The samples were kept in a crucible which was then placed in a one-end-closed quartz tube. To achieve efficient heat transfer, the sample loading was less than 50 mg. N₂ was purged from the other end of the tube to maintain the inert atmosphere. After 1 h of flushing at room temperature, the tube was quickly inserted to a tubular furnace in which the heating-zone temperature was 600 °C. To prevent the agglomeration of Ir atoms, the tube was quenched to room temperature after 1 min heat-treatment.

4. Electrochemical test procedure

We performed the electrochemical test using the classic 3-electrode setup. A Gamry Reference 600 potentiostat was employed, together with a Gamry RDE710 rotating electrode setup. Saturated calomel electrode (SCE, Gamry, USA) separated from the solution by a 10 cm bridge was used as a reference electrode, and a graphite rod (Gamry, USA) as a counter electrode. To prepare the ink, 1 mg of the catalyst, 1 ml ethanol and 10 μL Nafion® (D-521 dispersion 5 wt % in water/isopropanol, Alfa Aesar 42117) were mixed in a 10 ml vial and ultrasonicated overnight. The ink was dropcasted on to the glassy carbon rotating disc electrode (RDE, diameter=5 mm) by 5 μL × 6, with air drying in between. The total catalyst loading was 30 μg, or 153 μg/cm². The Ir loading on the RDE was therefore 0.81 μg/cm². RDE was polished sequentially by diamond polishing films

with 1 and 0.1 μm particles (Allied High Tech Products, USA) with water rinse before the catalyst deposition.

Both cyclic voltammetry (CV) and linear scan voltammetry (LSV) were performed in 0.1M KOH aqueous solutions with a scan rate of 10 mV s^{-1} and a rotating speed at 1600 rpm. Nitrogen (99.999%) or oxygen (99.999%) were bubbled for 30 minutes to saturate the electrolyte, and were flowed above the solution ('gas blanket') during the experiments. The solution resistance was determined initially (typically 30–50 Ohm). CV was performed between 0.8 to 1.2 V vs. RHE to measure the capacitive current for all the examined catalysts, and a post-measurement correction was applied. In the automatic iR correction, 95% of the value was used as a positive correction factor in the Gamry Framework and the obtained voltammogram was reported as it was. As a comparison, we also carried out post iR correction without using the automatic one from the software. The reported potential was calculated using the equation $E_r = E - iR$. Rotating ring-disk electrode (RRDE) measurements were performed on an E7R9 RRDE (Pine Instruments, USA) with a glassy carbon disk and platinum ring of area 0.2475 cm^2 and 0.1866 cm^2 , respectively. The standard collection efficiency was 37 %. However, we have re-measured it in-house using 10 mM $\text{K}_3[\text{Fe}(\text{CN})_6]$ in 0.1 M KCl solution and rotated under different rotation rates (400, 900, 1200, rpm). The disk potential was scanned from 0.4 V to -0.6 V vs. SCE while the ring potential was fixed to 0.5 V. In the OER measurement using RRDE, the electrolyte was saturated by N_2 and electrode rotating speed was set at 1600 rpm. The disk potential was scanned from 0 V to 0.7 V vs. SCE while the ring potential was fixed to -0.5 V vs. SCE to ensure the reduction of the evolved O_2 . The reported potentials in the "Results and discussion" were all vs. RHE using the equation below:

$$E(\text{RHE}) = E(\text{SCE}) + 0.242 + 0.059\text{ pH}$$

5. Materials characterizations

X-Ray diffraction (XRD) patterns were obtained using a MiniFlex II diffractometer equipped with $\text{CuK}\alpha$ radiation. The X-ray tube was operated at 30 kV and a current of 5 mA. Nitrogen adsorption isotherms were measured on a Thermo Scientific Surfer instrument at 77 K. The sample was dried in vacuum (1×10^{-3} mbar) for 3 h at 200 °C prior to the measurement. Fourier-transform infrared spectroscopy (FTIR) was carried out using a Thermal Fisher iS50 spectrometer. KBr pellet was used to record the spectra. Elemental analysis was performed using the inductively-coupled plasma atomic emission spectroscopy (PerkinElmer, Optima 4300DV). The samples after the electrochemical measurements were collected from the RDE. Scanning electron microscope (FEI Verios 60 with ETD detector) was used to observe the morphology of the samples. Transmission electron microscope (TEM) analysis was performed using a JEOL JEM-ARM200C TEM with aberration correction. X-ray photoelectron spectroscopy (XPS) was carried out using a Kratos AXIS equipped with a monochromatic Al $\text{K}\alpha$ X-ray source. The base pressure in the analytical chamber was maintained at 10^{-9} mbar. The obtained spectra were analyzed using the Thermo Avantage software calibrated to the C 1s binding energy of 285.0 eV. For curve fitting and deconvolution, a

Shirley-type background subtraction and a Gaussian-Lorentzian peak shape were applied. In the assignment of nitrogen functionalities, we avoided using the pyrrolic, because they are known to decompose at temperatures above 800 °C to either pyridinic or graphitic nitrogen.

6. Computational Methods

The DFT calculations were performed using the VASP package (version 5.3) [1] using the RPBE functional [2]. The MnO₂ (110) surface consisted of a (3×1) unit cell (24 Mn and 48 O atoms) with 4 layers where the bottom two layers were fixed. In the case of Ir(*cus*)-MnO₂, a Mn(*cus*) atom was replaced by an Ir atom and allowed to relax. Spin-polarized calculations were performed in all cases. Reported energies are those of the lowest energy spin state. The cutoff of plane-wave basis is set to 450 eV. A Monkhorst-Pack k-point grid was used to account for Brillouin-zone integration. The structural optimizations were performed using the conjugate gradient algorithm until the maximum force on any atom was below 0.05 eV Å⁻¹.

We used the Computational Hydrogen Electrode (CHE) method to model the OER catalyzed by MnO₂ [3,4]. In the CHE method, the energetics of H₂ (g) is used instead of (H⁺ + e⁻). The adsorption energies of *O, *OH and *OOH are calculated using the reaction energies obtained from the reactions:



The free energies of reactions (1-3) correspond to ΔG_O , ΔG_{OH} and ΔG_{OOH} . Zero point energy (ZPE) and entropy (TS) contributions to these free energies were taken from previous work. [3] From these free energies, we can compute the reaction energies for the OER process as:

$$\Delta G_1 = \Delta G_{OH} \quad (4)$$

$$\Delta G_2 = \Delta G_O - \Delta G_{OH} \quad (5)$$

$$\Delta G_3 = \Delta G_{OOH} - \Delta G_O \quad (6)$$

$$\Delta G_4 = 4.92 - \Delta G_{OOH} \quad (7)$$

A number of studies have shown ΔG_2 to be a good descriptor for volcano-type activity plots [3,5]. The overpotential is then computed as:

$$\eta_{OER} = \max(\Delta G_1, \Delta G_2, \Delta G_3, \Delta G_4) / e^- - 1.23 \text{ V} \quad (8)$$

Table S1. Selected bond lengths [Å] and angles [°] in complex **2**

Ir1-C1	2.239(3)	Ir1-C11	2.039(2)
Ir1-C2	2.241(2)	C11-N1	1.368(3)
Ir1-C3	2.149(3)	C11-N2	1.363(3)
Ir1-C4	2.142(3)	N1-C11-N2	103.1(2)
Ir1-C5	2.146(3)	N1-C11-Ir1	127.95(18)
		N2-C11-Ir1	127.81(18)

NOTE: see the bond label in Figure S2.

Table S2. The OER performance of selected Ir-containing catalysts.

Journal	Material	Overpotential at 10 mA cm ⁻² (V)	Tafel slope (mV dec ⁻¹)	Ir mass activity at 10 mA cm ⁻² (A mg _{Ir} ⁻¹)	Ref.
<i>This Work</i>	Ir-MnO _x /N-C	0.25	47	3.71	
<i>Chem. Mater.</i>	Ir@Co ₄ N NFs	0.336	94.5	0.34	[s1]
<i>ACS sustainable Chem. Eng.</i>	Co@Ir/NC- 10%	0.28	73.8	0.50	[s2]
<i>ACS Appl. Mater. Interfaces</i>	Ir/NC	0.265	35	n.g.	[s3]
<i>Journal of Energy Chemistry</i>	AuIr/C	0.395	n.g.	n.g.	[s4]
<i>ChemComm</i>	Ir-Cu	0.340	38	0.12	[s5]
<i>Int. J. Hydrogen Energy</i>	Ni-(Ebonex/Ir)	0.367	56.3	0.03	[s6]
<i>ACS Appl. Mater. Interfaces</i>	Ir/Ni oxide	0.264	31	0.47	[s7]
<i>J. Mat. Chem. A</i>	IrO ₂	0.380	47.7	0.01	[s8]
<i>Electrochimica Acta</i>	IrO ₂ nanorod	ca. 0.43	n.g.	n.g.	[s9]
<i>J. Mat. Chem. A</i>	IrO _x -Hemin	0.35	n.g.	n.g.	[s10]
<i>ACS Catal.</i>	IrO ₂ /C	n.d.	64	<0.01	[s11](acid)
<i>Nat. Commun.</i>	6H-SrIrO ₃	0.248	n.g.	0.07	[s12](acid)

Notes:

(1) n.d.: not given or not deducible from the reference.

(2) References:

[s1] S.-H. Cho, K. R. Yoon, K. Shin, J.-W. Jung, C. Kim, J. Y. Cheong, D.-Y. Youn, S. W. Song, G. Henkelman, I.-D. Kim, *Chem. Mater.* **2018**, *30*, 5941–5950.[s2] D. Li, Z. Zong, Z. Tang, Z. Liu, S. Chen, Y. Tian, X. Wang, *ACS Sustain. Chem. Eng.* **2018**, *6*, 5105–5114.[s3] H. Wang, M. Ming, M. Hu, C. Xu, Y. Wang, Y. Zhang, D. Gao, J. Bi, G. Fan, J.-S. Hu, *ACS Appl. Mater. Interfaces* **2018**, *10*, 22340–22347.[s4] L. Yuan, Z. Yan, L. Jiang, E. Wang, S. Wang, G. Sun, *J. Energy Chem.* **2016**, *25*, 805–810.[s5] J. Pei, J. Mao, X. Liang, C. Chen, Q. Peng, D. Wang, Y. Li, *Chem. Commun.* **2016**, *52*, 3793–3796.[s6] B. M. Jović, U. Č. Lačnjevac, V. D. Jović, L. Gajić-Krstajić, J. Kovač, D. Poleti, N. V. Krstajić, *Int. J. Hydrog. Energy* **2016**, *41*, 20502–20514.[s7] L. Gong, D. Ren, Y. Deng, B. S. Yeo, *ACS Appl. Mater. Interfaces* **2016**, *8*, 15985–15990.

- [s8] S. Jung, C. C. L. McCrory, I. M. Ferrer, J. C. Peters, T. F. Jaramillo, *J. Mater. Chem. A* **2016**, *4*, 3068–3076.
- [s9] J. Ahmed, Y. Mao, *Electrochimica Acta*, **2016**, *212*, 686-693.
- [s10] P.-Y. Liu, C.-C. Hsu, M.-C. Chuang, *J. Mater. Chem. A* **2017**, *5*, 2959–2971.
- [s11] T. Reier, M. Oezaslan, P. Strasser *ACS Catal.* **2012**, *2*, 1765-1772.
- [s12] L. Yang, G. Yu, X. Ai, W. Yan, H. Duan, W. Chen, X. Li, T. Wang, C. Zhang, X. Huang, J. Chen, X. Zou *Nat. Commun.* **2018**, *9*, 5236.

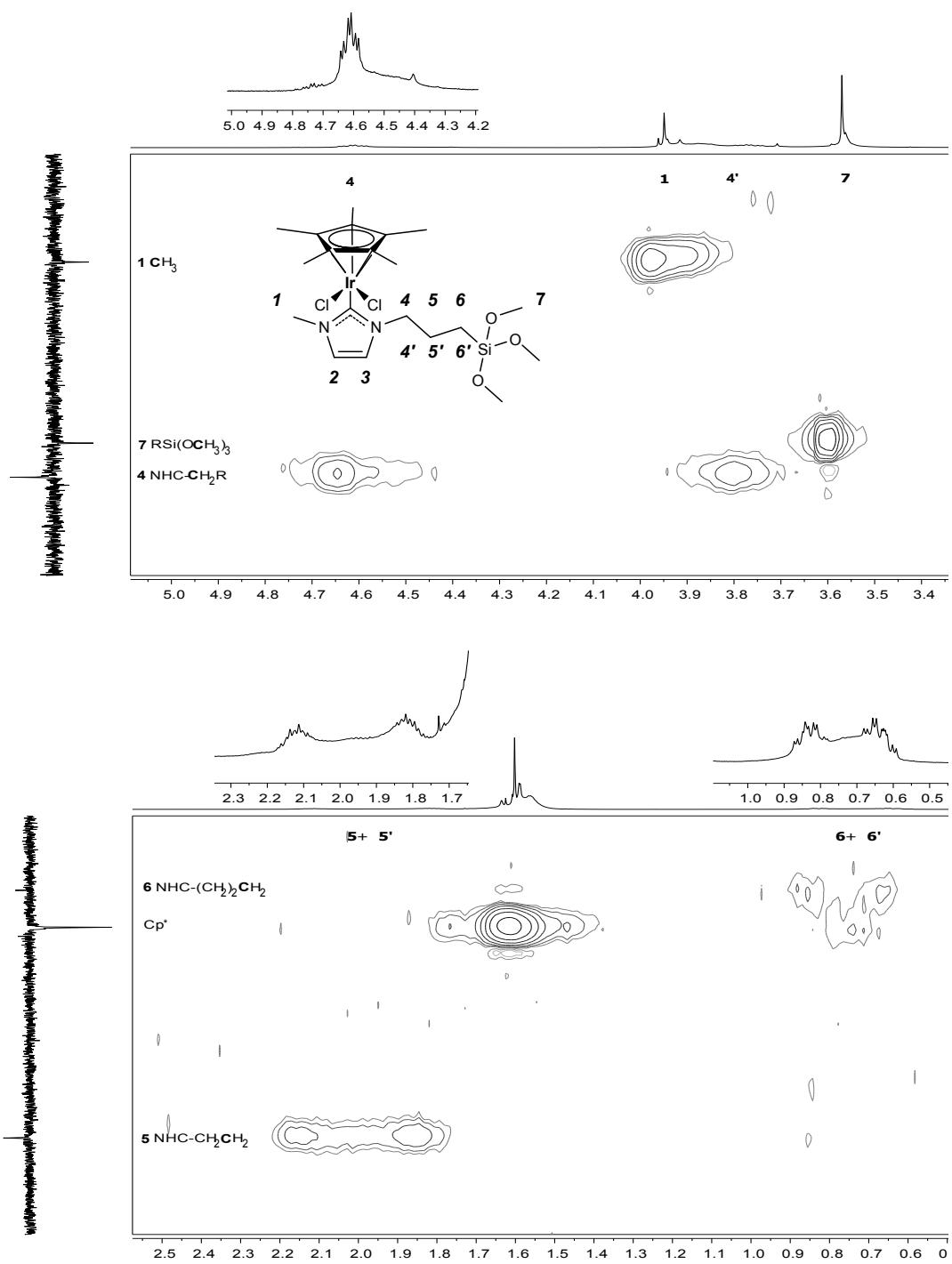


Figure S1. $^1\text{H}/^{13}\text{C}$ -APT HMQC spectrum of complex **2** in CDCl_3 .

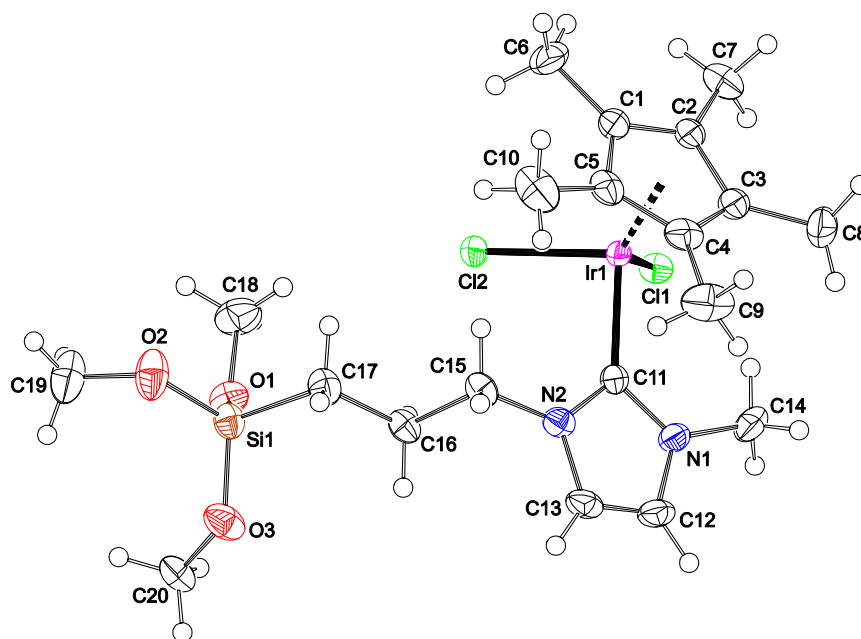


Figure S2. Displacement ellipsoid plot of complex **2** in the crystal (50% probability level).

$C_{20}H_{35}Cl_2IrN_2O_3Si$, Fw = 642.69, yellow needle, $0.37 \times 0.16 \times 0.10 \text{ mm}^3$, orthorhombic, $P2_12_12_1$ (no. 19), $a = 8.6297(3)$, $b = 15.3157(5)$, $c = 18.4968(6) \text{ \AA}$, $V = 2444.72(14) \text{ \AA}^3$, $Z = 4$, $D_x = 1.746 \text{ g/cm}^3$, $\mu = 5.75 \text{ mm}^{-1}$. 41172 Reflections were measured on a Bruker Kappa ApexII diffractometer with sealed tube and Triumph monochromator ($\lambda = 0.71073 \text{ \AA}$) at a temperature of 150(2) K up to a resolution of $(\sin \theta/\lambda)_{\text{max}} = 0.65 \text{ \AA}^{-1}$. The intensities were integrated with the Saint software. Multiscan absorption correction and scaling was performed with SADABS (correction range 0.52-0.75). 5598 Reflections were unique ($R_{\text{int}} = 0.019$), of which 5418 were observed [$I > 2\sigma(I)$]. The structure was solved with Direct Methods using SHELXS-97. Least-squares refinement was performed with SHELXL-97 against F^2 of all reflections. Non-hydrogen atoms were refined freely with anisotropic displacement parameters. Hydrogen atoms were introduced in calculated positions and refined with a riding model. 272 Parameters were refined with no restraints. $R1/wR2$ [$I > 2\sigma(I)$]: 0.0129 / 0.0306. $R1/wR2$: 0.0143 / 0.0313. $S = 1.084$. Flack parameter $x = -0.017(3)$. Residual electron density between -0.44 and 0.85 e/\AA^3 . Geometry calculations and checking for higher symmetry was performed with the PLATON program.

CCDC 1521805 contains the supplementary crystallographic data for this paper. These data can be obtained free of charge from The Cambridge Crystallographic Data Centre via www.ccdc.cam.ac.uk/data_request/cif.

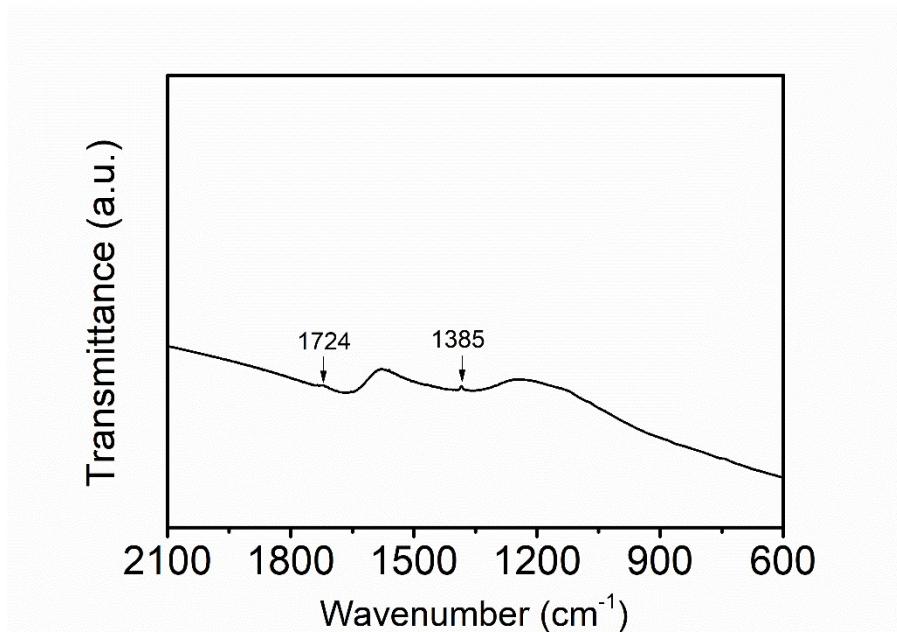


Figure S3. FTIR spectra of MnO_x/N-C after removing MnO_x through acid-washing.

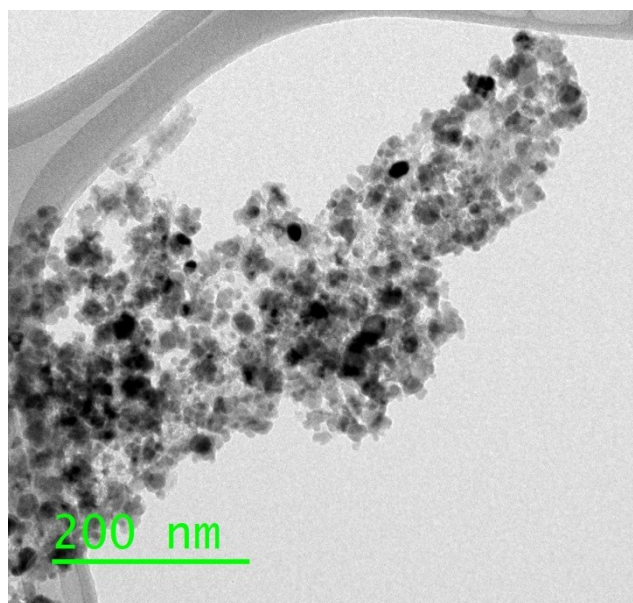


Figure S4. TEM micrograph of Ir-MnO_x/N-C.

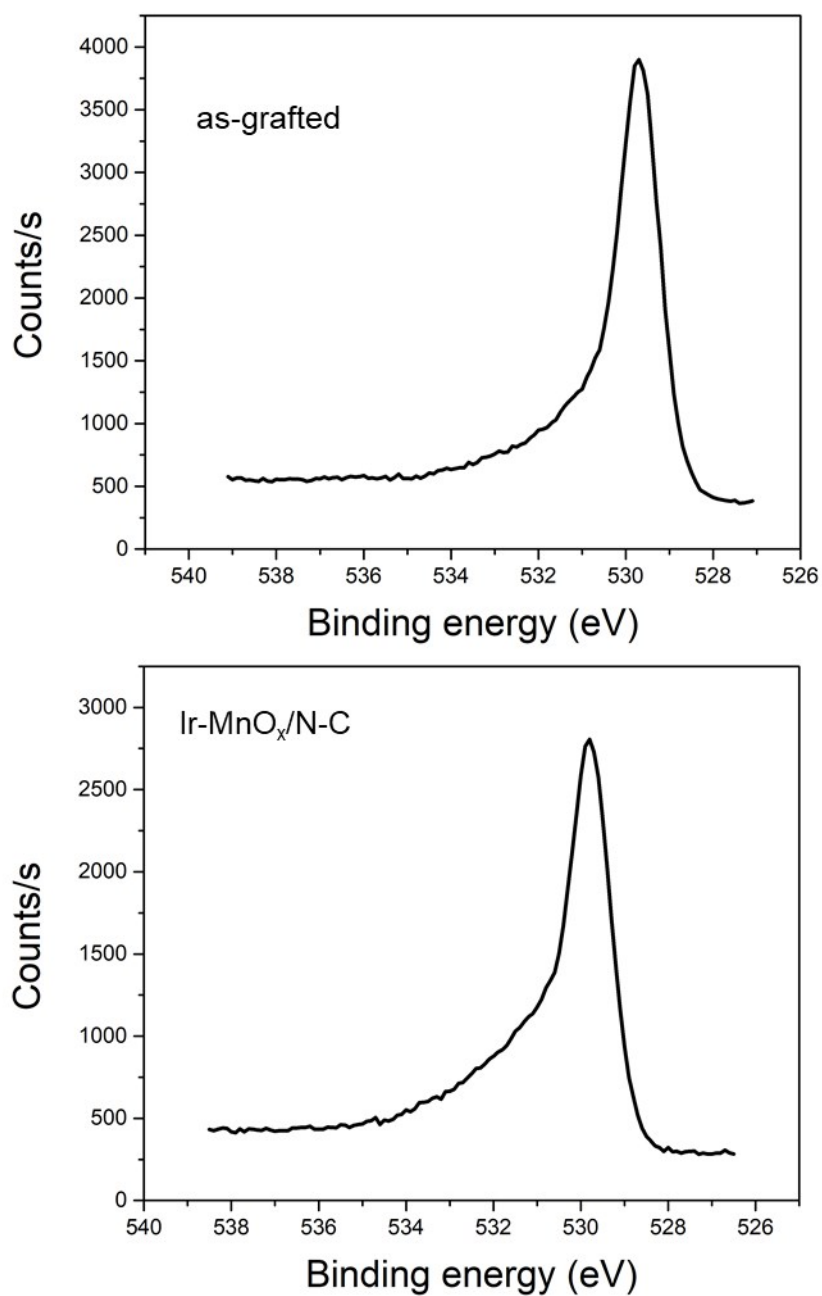


Figure S5. XPS spectra of O 1s core level, the top spectrum is MnO_x/N-C after grafting complex 2 but before pyrolysis, the bottom is Ir-MnO_x/N-C.

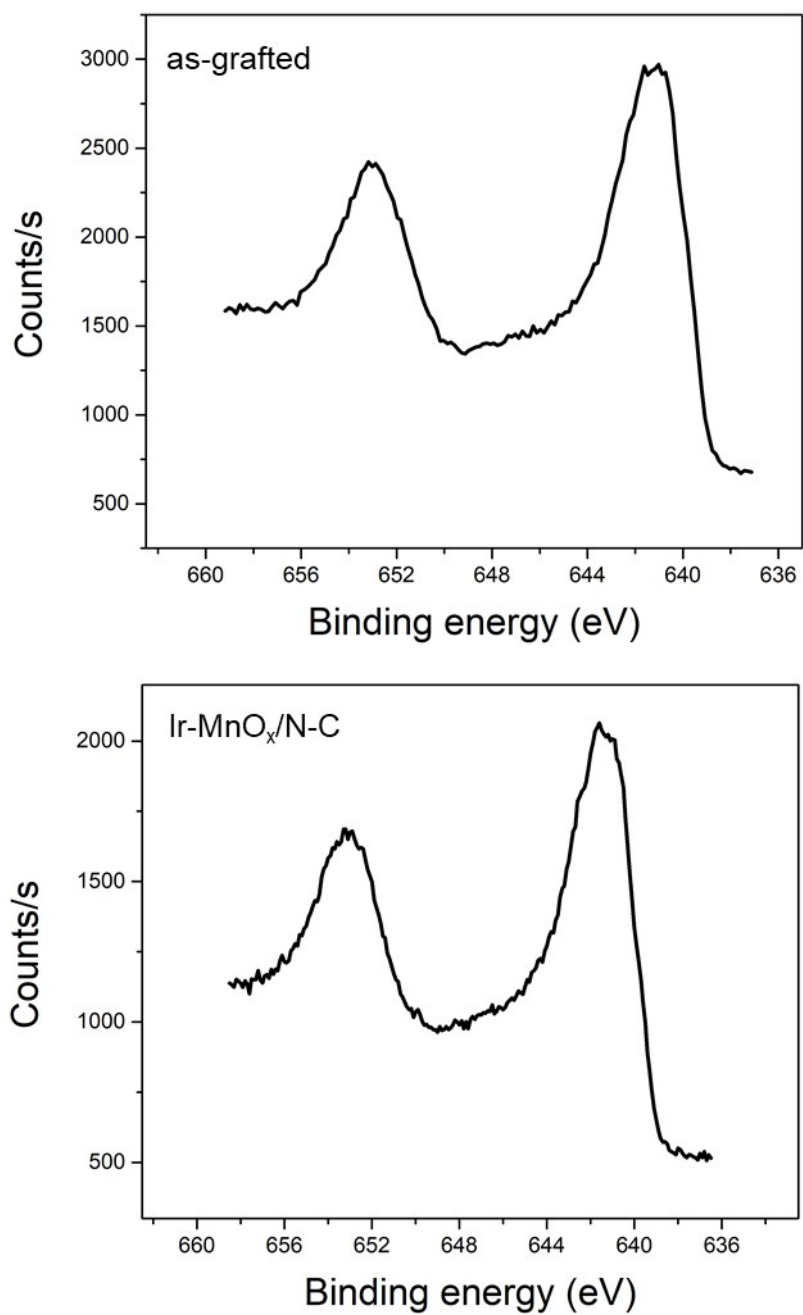


Figure S6. XPS spectra of Mn 2p core level, the top spectrum is MnO_x/N-C after grafting complex 2 but before pyrolysis, the bottom is Ir-MnO_x/N-C.

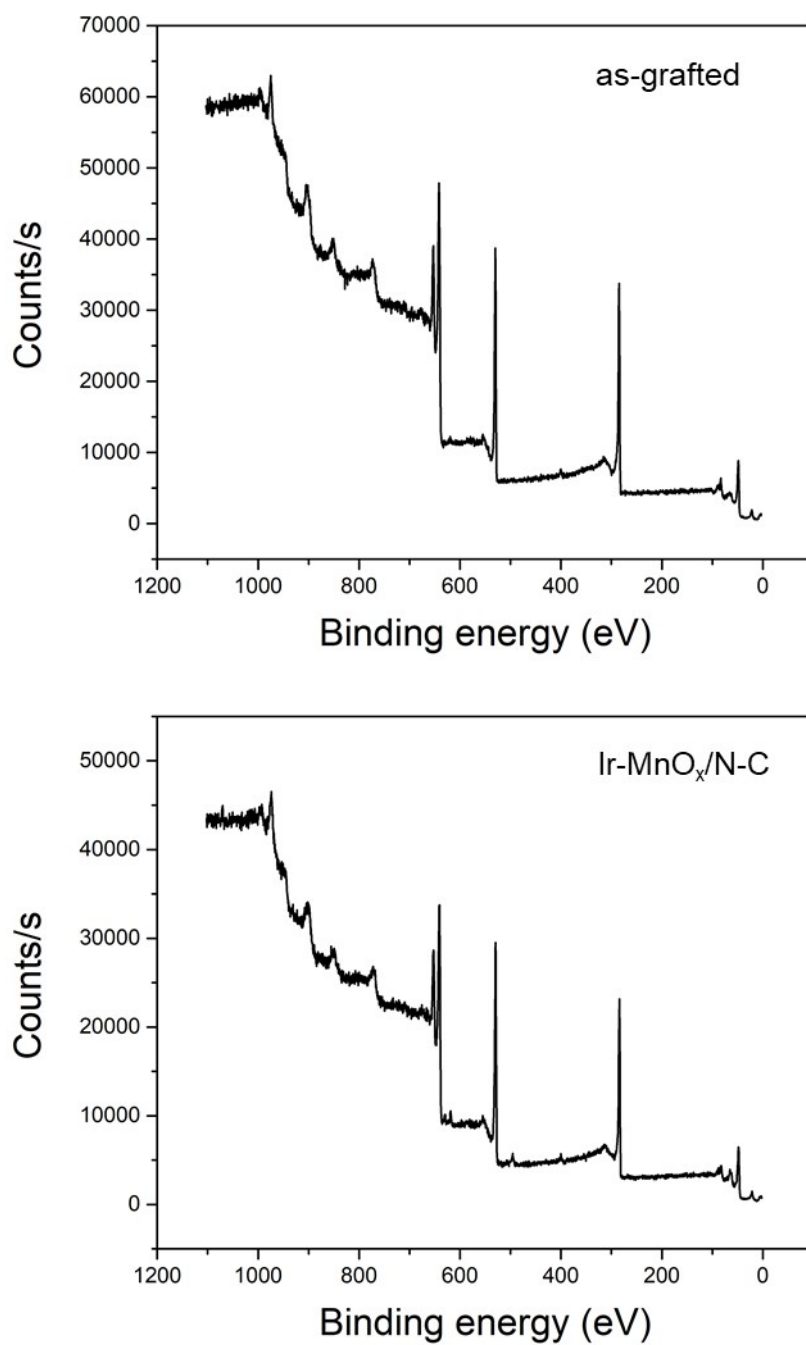


Figure S7. XPS survey spectra, the top spectrum is MnO_x/N-C after grafting complex 2 but before pyrolysis, the bottom is Ir-MnO_x/N-C.

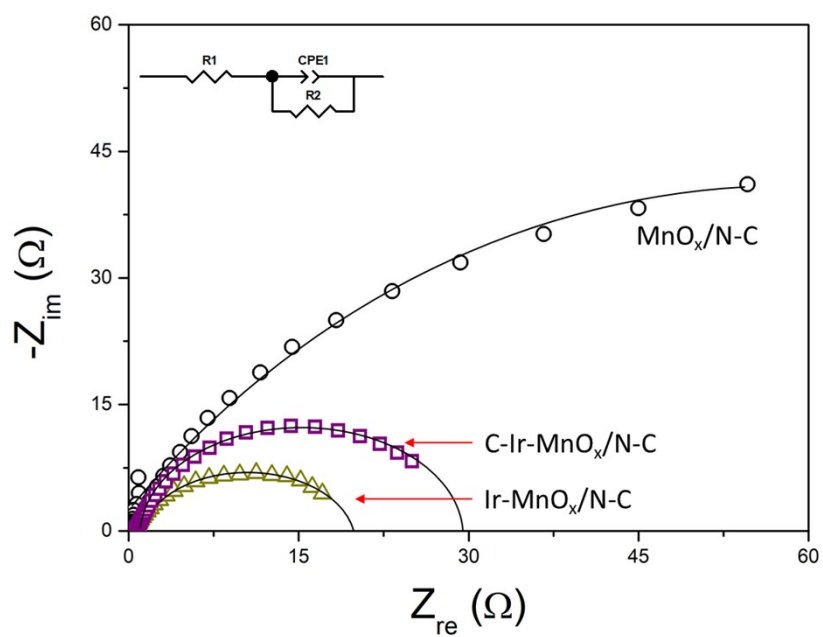


Figure S8. The Nyquist plots (symbol) and the fitted curves derived from the equivalent circuit (solid line) from the EIS measurement of MnO_x/N-C, C-Ir-MnO_x/N-C and Ir-MnO_x/N-C. The cells are all biased at 1.5 V vs. RHE.

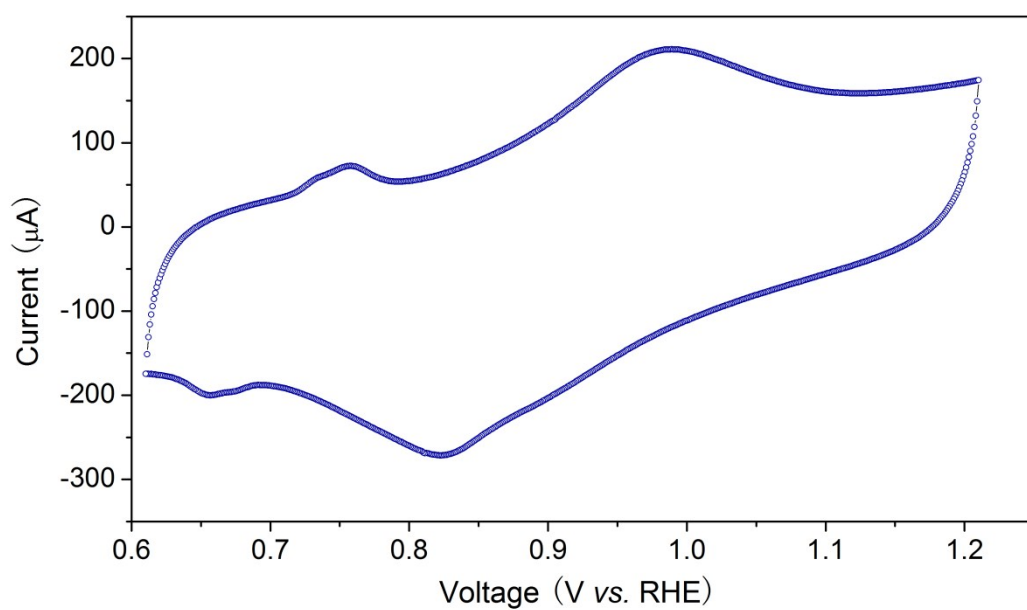


Figure S9. Cyclic voltammogram of Ir-MnO_x/N-C in N₂-saturated 0.1M KOH, the scan rate was 10 mV/s.

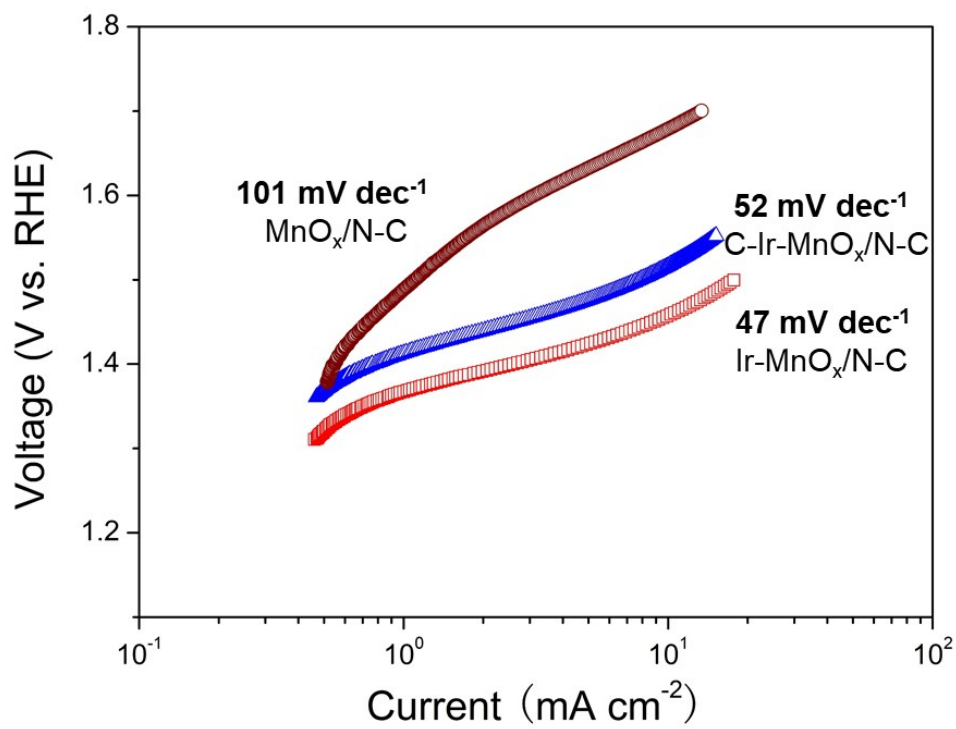


Figure S10. Tafel plots of MnO_x/N-C, C-Ir- MnO_x/N-C and Ir- MnO_x/N-C.

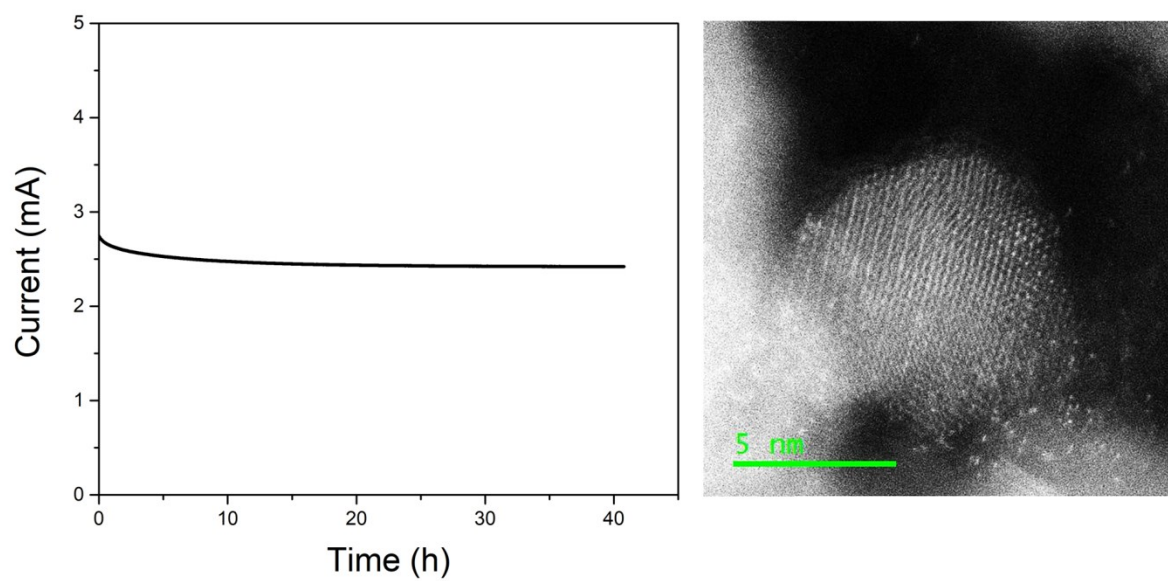


Figure S11. (Left) the chronoamperogram of Ir-MnO_x/N-C in O₂-saturated 0.1M KOH at 1.5 V, the RDE was rotating at 300 rpm. (right) the HAADF image of Ir-MnO_x/N-C after the longevity test.

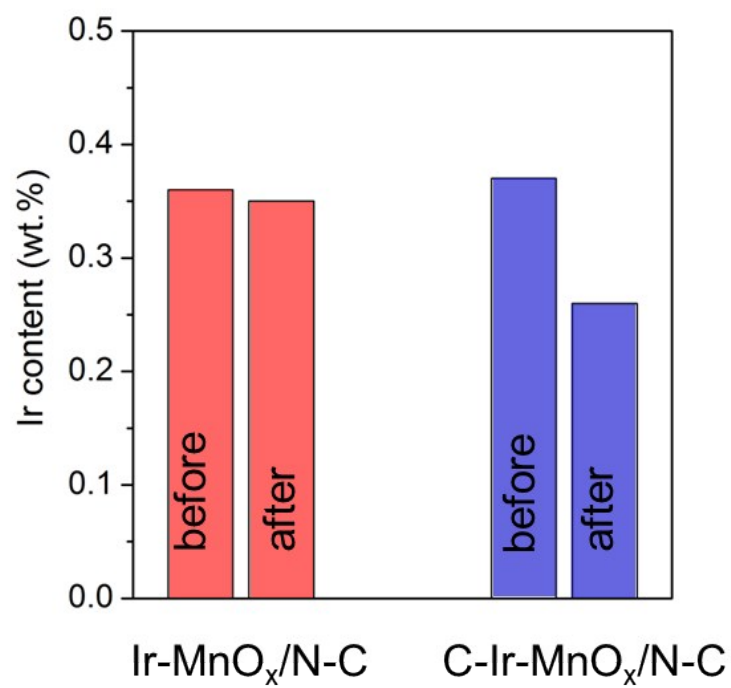


Figure S12. Ir content comparison of Ir-MnO_x/N-C and C-Ir-MnO_x/N-C before and after 100 CV cycles (1~1.6 V vs. RHE).

References

- [1] G. Kresse, J. Furthmüller, *Phys. Rev. B* 1996, **54**, 11169–11186.
- [2] B. Hammer, L. B. Hansen, J. K. Nørskov, *Phys. Rev. B* 1999, **59**, 7413–7421.
- [3] I. C. Man, H.-Y. Su, F. Calle-Vallejo, H. A. Hansen, J. I. Martínez, N. G. Inoglu, J. Kitchin, T. F. Jaramillo, J. K. Nørskov and J. Rossmeisl, *ChemCatChem*, 2011, **3**, 1159–1165.
- [4] H.-Y. Su, Y. Gorlin, I. C. Man, F. Calle-Vallejo, J. K. Nørskov, T. F. Jaramillo, and J. Rossmeisl, *Phys. Chem. Chem. Phys.*, 2012, **14**, 14010-14022.
- [5] Z. W. Seh, J. Kibsgaard, C. F. Dickens, I. Chorkendorff, J. K. Nørskov and T. F. Jaramillo, *Science*, 2017, **355**